

**2004**  
**NASA FACULTY FELLOWSHIP PROGRAM**

**MARSHALL SPACE FLIGHT CENTER**  
**THE UNIVERSITY OF ALABAMA**  
**THE UNIVERSITY OF ALABAMA IN HUNTSVILLE**  
**ALABAMA A&M UNIVERSITY**

**THE PLUNGE PHASE OF FRICTION STIR  
WELDING**

Prepared by:	John C. McClure
Academic Rank:	Professor
Institution and Department:	University of Texas El Paso, Metallurgical and Materials Engineering Department
NASA/MSFC Directorate:	Engineering
MSFC Colleague:	Dr. Arthur Nunes

## **Introduction**

The many advantages of Friction Stir Welding<sup>1</sup> have led to a relatively rapid acceptance in the often conservative welding community<sup>2, 3</sup>. Because the process is so different from traditional fusion welding, with which most investigators are most familiar, there remain many aspects of FSW for which there is no clear consensus.

For example, the well known onion rings<sup>4</sup> seen in transverse sections have been variously interpreted as grain size variations<sup>5</sup>, variation in density of second phase particles<sup>6</sup> and parts of the “carousel” of material rotating with the pin that have been shed from the carousel<sup>7</sup>. Using Orientation Imaging Microscopy, Schneider<sup>8</sup> has recently noted that the onion rings have a different orientation (and hence etch differently) than the surrounding material, and this orientation is consistent with slip plane orientations at the edge of the carousel.

Likewise, the forces and torque exerted by the FSW tool on the work piece largely remain unaccounted for. Although these forces are routinely measured by investigators with commercial instrumented welders, they are rarely reported<sup>9</sup> or even qualitatively analyzed.<sup>10</sup>

This paper will introduce a model based on a “carousel” or disk of material that rotates with the tool to estimate the torque and plunge force required to plunge a tool into the work piece. A stationary tool is modeled rather than the moving tool because effects such as thermal transients and metallurgical changes in the sample (primarily aging in aluminum) can be more easily accounted for. It is believed, however, that with some modifications the model should be applicable to a moving tool also.

## **Experimental Procedure**

Plunging penetrations were made on the horizontal weld tool at Marshall Space Flight Center on 2219 aluminum (nominal composition 6.3 % Cu, .3% Mn balance aluminum). The work piece was 0.40in (1.0 cm) thick. The pin tool was threaded (20/in or 7.8/cm) and was 0.490 in (1.24cm) in diameter and .375 in. (0.95cm) long with a flat bottom. The tool shoulder was 1.20 in. (3.0 cm) in diameter and slightly concave to the work piece. Penetrations were made to various plunge depths, measured from the tip of the pin, of 0.1 in (0.25 cm) to 0.388 in (0.98cm). The latter plunge submerged the shoulder and is typical of the plunge that would have been used to make a weld. After the desired plunge depth was attained, the welder was emergency stopped to freeze the pin in the sample. The sample was then unscrewed from the pin to preserve the structure.

Plunge speeds were 0.1 in/min or 0.2 in/min (0.0042 to .0084 cm/sec) and the tool rotational speed was varied from 200 rpm to 400 rpm with most plunges made at 300 rpm. Motor torque, plunge force, and plunge depth were recorded during the experiment.

Samples were cut, polished, and etched with Keller’s Solution for metallographic inspection.

## Results and Discussion

Fig. 1 shows plunge force versus plunge depth for 200 rpm, 300 rpm, and 400 rpm plunges all made at 0.1 in/min (0.042 cm/sec). Also included is a plunge at 300 rpm made twice as fast at 0.2 in/min. (0.0084 cm/min).

The cooler welds (made at 200 rpm and the fast plunge at 300 rpm) require the greatest plunge force because they have undergone the least heating and the weld metal has the highest flow stress. The first thin piece of extruded metal (seen on the left side of Fig. 2) does not appear until a plunge depth of approximately 0.07 in. Beyond this depth, all plunge forces decreased or remained nearly constant (in the case of the 400 rpm sample) as thermal equilibrium was established and material properties stabilized and flow stress decreased. Thus, only the 400 rpm sample exhibited steady state behavior and will be the focus of this work.

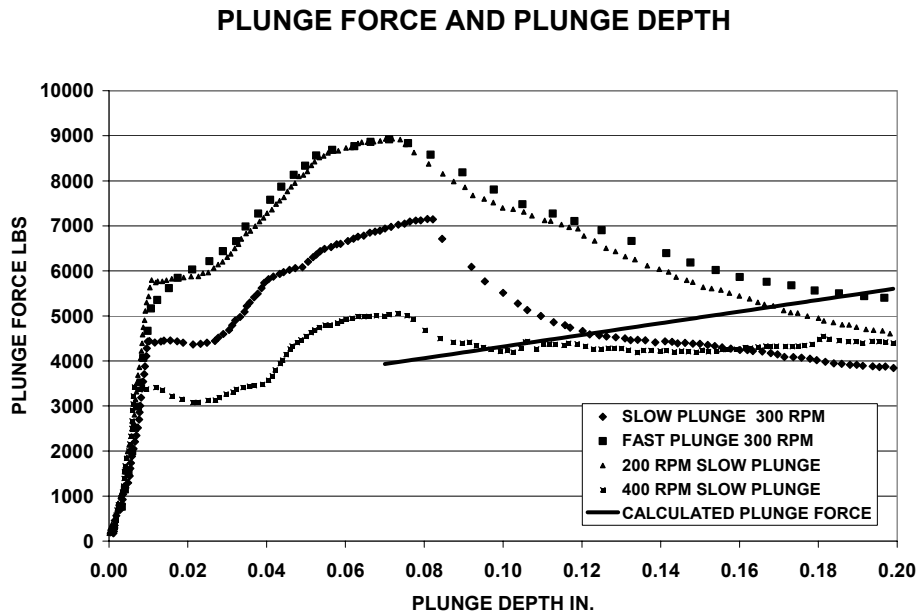


Figure 1: Plunge force versus plunge depth for plunges of 200, 300, and 400 rpm all made at 0.10 in/min. Also shown is a plunge at 300 rpm made twice as fast at .20 in/min. Note that the 400 rpm sample has approximately constant plunge force beyond .08 in. The Calculated Plunge Force is discussed later and should be compared to the 400 rpm data at plunges greater than 0.08 in.

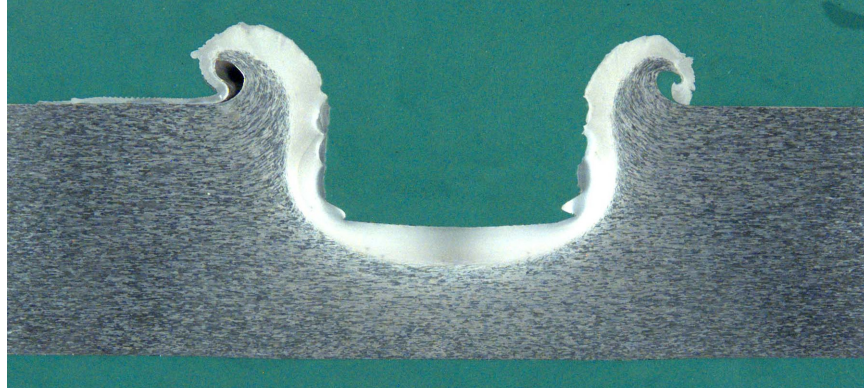
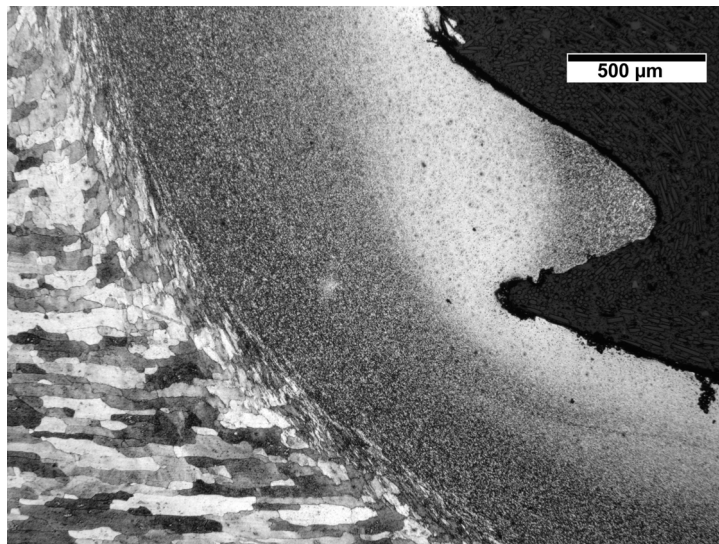
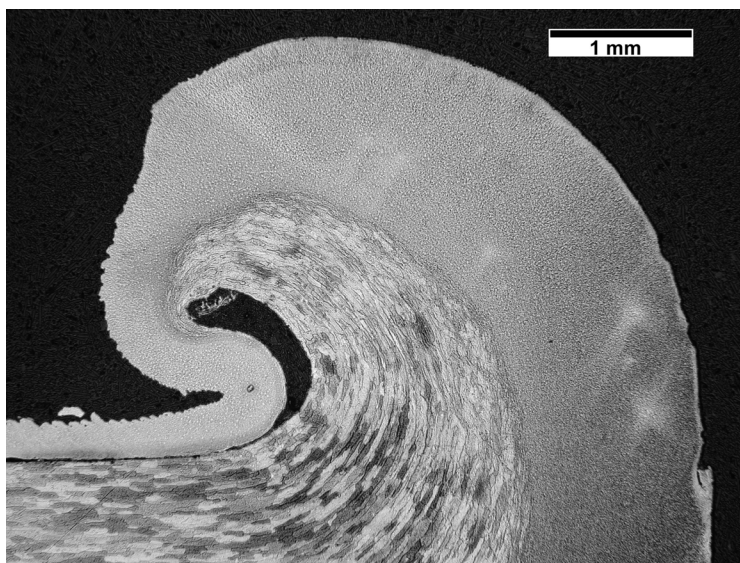


Figure 2: Low magnification cross section of sample plunged to 0.2 inches. Note light etching material surrounding pin fossil some of which is extruded onto the surface. The thin “tail” of metal seen on left side of pin fossil was the first part extruded. Sample is 0.40 in thick.

Fig. 2 shows a low magnification micrograph of the 400 rpm sample after the pin tool was stopped and removed. It is seen that the pin fossil is surrounded by a shiny, fine grained region of recrystallized grains. This is similar to the carousel<sup>7,11</sup> seen on fully plunged welds. Fig. 3 shows higher magnification micrographs of regions around the weld fossil.





**Figure 3: Higher magnification micrographs of Fig. 2 showing lower corner of fossil (above) and extruded material on left side. Note both deformed unrecrystallized grains and fine recrystallized grains that have been extruded by the tool. The fine grains are equiaxed and about 5 microns in size.**

The “tail” seen on the left side of Fig. 3 bottom is the first material extruded as the tool is plunged and is a record of the thickness of the fine grained region as plunge advanced. This material is easily seen by the welder during plunge and does not rotate with the tool.

Fig. 4 shows the pin tool torque (not motor torque) as a function of weld depth. Again the 400 rpm sample shows approximately depth independent torque after 0.07 inches of plunge and appears to be at steady state. The other cooler samples require more torque, and the slope of their curves decreases as temperature increases because steady state conditions are reached more rapidly by the hotter samples. The initial rapid increase in torque (Fig. 4) and plunge force (Fig. 1) below 0.01in of plunge is thought to be of mechanical origin as the welder engages the work piece.

## TORQUE VERSUS PLUNGE DEPTH

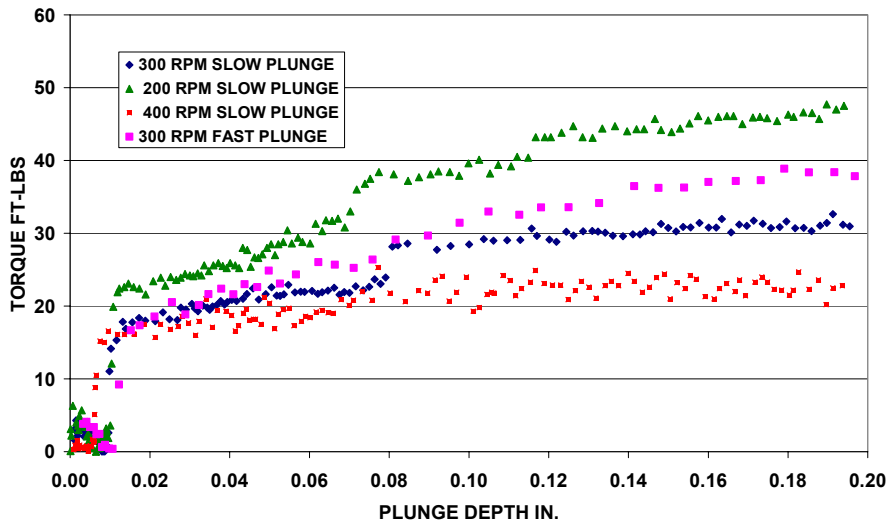


**Figure 4: Measured torque during plunge for various rotational rates and plunge speeds.**

The metal flow configuration around the initially penetrating friction stir welding tool is sketched in Figure 5. The fine grained material seen surrounding the pin tool fossil in Fig. 2 is evidence that material has undergone a very large deformation to promote this recrystallization. According to the model presented in this work, all this deformation takes place in a circular disk of material below the pin tool. This disk rotates with the pin tool and accretes material into the disk as the pin tool plunges. At the same time, material is squeezed out from the edges of this disk and rises along the sides of the pin tool. Only the region directly below the pin tool actually rotates. As mentioned above, material extruded during weld is seen to remain fixed to the work piece and does not rotate with the tool.

That there is a shear surface (the plane dividing the recrystallized and non-recrystallized material) below the tool is apparent from the sharply defined onset of recrystallized metal below the tool. This surface seen in Figure 2 is curved, but for simplicity will be represented as flat. Note that shear between rotating disk below the pin takes place between the rotating disk and the non-recrystallized material both on the flat surface of the disk and on its curved outer periphery.

As the tool descends the shear surface descends, and metal enters the rotating disk to be recrystallized and squeezed out at the sides and up along the tool to the free surface. In Figure 2 the extruded annular cylinder has roughly the same thickness as the rotating plug of metal and comprises chiefly recrystallized metal. The extruded cylinder does not rotate, at least at the upper surface, where it can be observed. It is assumed that the lower

threads deflect the upward flow so that contact between metal and tool is limited and negligible on the inside (the side against the pin tool) of the annular cylinder.

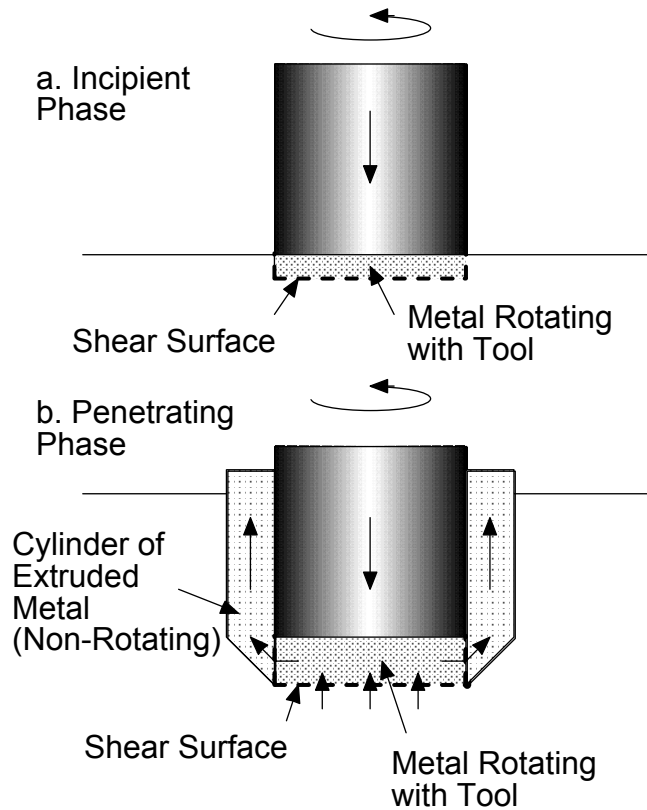


**Figure 5: Idealization of weld metal flow configuration in the vicinity of the penetrating friction stir tool.**

The shear stress  $\tau$  opposing motion at a shearing interface is a function of temperature and strain rate. To simplify the analysis, we will assume that the temperature is the same over all the shearing surfaces. The spindle torque  $M$  can be roughly estimated according to the relation:

$$M = \int_0^R 2\pi r^2 \tau dr + 2\pi R^2 h \tau = \frac{2\pi R^3}{3} \left( 1 + 3 \frac{h}{R} \right) \tau \quad (1)$$

$M$  is the torque,  $R$  is the pin tool radius,  $h$  is the thickness of the rotating disk, and  $\tau$  is the shear stress of the material.

The first term comes from torque due to motion of the flat circular face of the disk and the second term comes from shear between the circumference of the disk and the surrounding material. If  $R$  is 0.25-inches and  $h/R$  is approximately 0.3 (from Figure 2) then for the steady state torque of 22.5 ft-lbs of the 400 rpm data in Fig. 4,  $\tau$  is approximately 4,500 psi. (31 Mpa).

Colder penetrations (lower RPM and faster plunge speeds) show some increase in torque with penetration depth as well as the anticipated higher  $\tau$ . This is thought to be due to

increased friction between tool and work piece at the threads. Colder and harder material is more difficult to deflect from the threads. In situations where the rise in torque with penetration is greater, the imprint of the threads in sections such as shown in Figure 2 is more defined.

There are several forces that the pin tool must overcome in order to penetrate. In particular, the plunge force must be able to squeeze the material in the rotating disk below the pin out to the sides. This requires overcoming a radial shear force between the pin tool and the disk as well as expanding the disk itself which requires overcoming a hoop force within the disk. An additional force is required to bend the disk around the corner of the tool so that it can rise. Lastly, the force necessary to push the material upward along the shear surface between the cylindrical annulus of recrystallized material and the parent metal must be supplied.

To calculate the plunge force, free body diagrams with stresses (not forces) are shown in Figure 6 which permits a calculation of the plunge force  $F_z$ . This Vertical equilibrium on the annular extruded cylinder requires that

$$\pi [(R+h)^2 - R^2] P_1 = 2\pi(R+h)\delta\tau \quad (2a)$$

or

$$P_1 = 2 \left( \frac{1 + \frac{R}{h}}{1 + 2\frac{R}{h}} \right) \frac{R}{h} \frac{\delta}{R} \tau \quad (2b)$$

Equilibrium of the corner element requires

$$P_2 \left( \frac{1}{\sqrt{2}} \right) = P_1 \left( \frac{1}{\sqrt{2}} \right) + \sqrt{2} \tau \quad (3)$$

or

$$P_2 = P_1 + 2\tau = 2\tau \left[ 1 + \left( \frac{1 + \frac{R}{h}}{1 + 2\frac{R}{h}} \right) \frac{R}{h} \frac{\delta}{R} \right] \quad (4)$$

Equilibrium of a ring element of radius  $r$ , height  $h$  and thickness  $dr$  of the cylindrical plug of metal requires:

$$2rhdP = -2(2\tau)hdr - 2r(2\tau dr) \quad (5)$$

The first term on the right is the plastic hoop stress; the second, shear resistance to flow at the bottom surface of the disk. Hence

$$P = P_2 + 2\tau \ln \frac{R}{r} + 2\tau \left(1 - \frac{r}{R}\right)$$

This pressure must be integrated over the area of the disk to obtain a force.

$$F_z = \int_0^R 2\pi r \left[ P_2 + 2\tau \ln \frac{R}{r} + 2\tau \left(1 - \frac{r}{R}\right) \right] dr$$

$$= 2\pi R^2 \left( \frac{1}{2} P_2 + \frac{5}{6} \tau \right) = 2\pi R^2 \tau \left[ \frac{11}{6} + \left( \frac{1 + \frac{R}{h}}{1 + 2\frac{R}{h}} \right) \frac{R}{h} \frac{\delta}{R} \right] \quad (7)$$

(6)

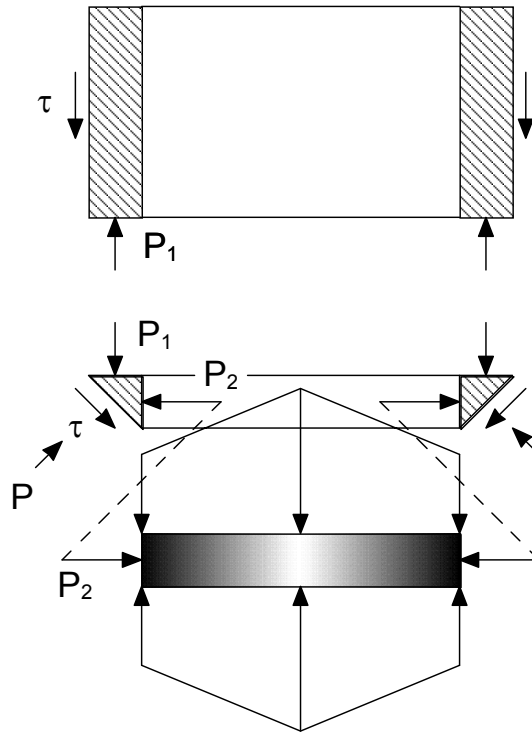


**Figure 6: Free body diagrams for flow elements in the vicinity of the penetrating friction stir tool.**

If the same value of shear stress calculated from the torque (4500 psi) is inserted in (7) a value of plunge force in good agreement with experimental results is obtained. See “Calculated Plunge Force” in Fig. 1.

Note that if  $h$  (the thickness of the recrystallized disk) is very small, the second term in Eq. 7 can dominate and the plunge force will be dependent on the plunge distance,  $\delta$ . Such dependence is seen from 0.01 inch plunge to 0.08 inch in Fig. 1. The material extruded in the “tail” seen in Fig. 2 is only 0.001 in. (0.0025 cm) thick and is probably

representative of the thickness of the rotating disk in the early stages of plunge, so the sharp increase at low plunges in Fig. 1 is not unexpected.

### **Conclusions**

1. The FSW plunge phase torque is that required to rotate a disk of material which rotates with the pin directly below it.
2. This disk is formed of recrystallized metal that was deformed by the pin tool abrasion against the parent metal. As plunge continues, more material is added to this layer until an equilibrium thickness sets in after about .08 in. of plunge.
3. The plunge force required in FSW is the force needed to deform in an outward direction this disk so that it can rise along the pin and eventually be expelled at the surface of the work piece.
4. The shear stress calculated from torque measurements and separately from plunge force measurements agree quite well, and is typical of metals a few hundred degrees below their melting point.

---

<sup>1</sup> W.M. Thomas, E.D. Nicholas, L.C. Needham, M.G. Murch, P. Templesmith, and J.C. Dawes: International Patent Application No. PCT/GB92/02203; G.B. Patent Application No. 9125978.8, 1991 and U.S. Patent No. 5,460,317, 1995.

<sup>2</sup> O.T. Midling, J.S. Kvale, and O. Dahl, *Proc. 1<sup>st</sup> Int. Symposium on Friction Stir Welding*, Thousand Oaks, CA, June 1999.

<sup>3</sup> The Welding Institute web site keeps a current list of applications. See [http://www.twi.co.uk/j32k/unprotected/band\\_1/fswapp.html](http://www.twi.co.uk/j32k/unprotected/band_1/fswapp.html)

<sup>4</sup> K.N. Krishnan, *Mater. Sci. Eng.*, 2002, Vol. A327, pp. 246-251.

<sup>5</sup> H. Jin, S. Saimoto, M. Ball, P.L. Threadgill, *Mat. Sci. and Tech.*, 2001, vol 17, pp 1605-1614.

<sup>6</sup> M.A. Sutton, B. Yang, A.P. Reynolds, Taylor, R., *Mat. Sci. & Engr.*, Vol. A323, 2002, pp. 160-166.

<sup>7</sup> Guerra, M., *op cit.*

<sup>8</sup> J.A. Schneider, A.C. Nunes Characterization of Plastic Flow and Resulting Micro Textures in Friction Stir Welds, *Mat. & Met. B*, April 2004.

<sup>9</sup> Tang, W., *op cit*

<sup>10</sup> M. Melendez, J.C. McClure, A. Nunes, "Forces During Friction Stir Welding", International Materials Conference, Cancun, Mexico, 2002.

<sup>11</sup> Coronado, E., "Effect of Pin Tool Shape on Friction Stir Welds" M.S. Thesis, University of Texas El Paso, 2002.